Quantum Cascade Laser integrated with metal-dielectric-metal plasmonic antenna

Dibyendu Dey, Ryan. M. Gelfand, John Kohoutek, Alireza Bonakdar and Hooman Mohseni[1]

Department of Electrical Engineering and Computer Science

Northwestern University, Evanston, Illinois, USA

ABSTRACT

In the near field region, optical antennas can generate local hot spots with high energy density. It can be very useful in increasing the photon-matter interactions for bio-sensing applications. There are several important bio-molecules having signature frequency (vibrational resonance) matching the mid infrared region of the optical spectrum. Thus mid-infrared antenna integrated with Quantum cascade laser (QCL) is highly desirable as it is currently considered to be one of the most efficient mid-infrared laser sources with a huge gamut of commercial applications. Here, we present a novel metal-dielectric-metal (MDM) based plasmonic nanorod antenna integrated on the facet of a room temperature working Quantum Cascade Laser. Simulations showed that at an optimized SiO_2 thickness of 20nm, the antenna can generate a local electric field with intensity 500 times higher than the incident field intensity. Further, it can increase the number of regions with local hot spots due to a higher number of geometrical singularities or sharp edges present in the MDM structure. This feature can be extremely useful, especially for bio-sensing applications. All device structures have been optimized based on 3d finite-difference time-domain (FDTD) numerical simulations. The antenna was fabricated on the facet of QCL using focused ion beam (FIB). The integrated plasmonic QCL has been measured using an apertureless mid-infrared near field scanning optical microscopy (a-NSOM). The measurement set-up is based on an inverted microscope coupled with a commercially available Atomic Forced Microscopy (AFM). We have experimentally found that such integrated nano antenna can generate a very narrow optical spot size, much below the diffraction limit, with high power density that matches well with the simulation results.

Key words: Bio-sensing, Focused ion beam milling, Field enhancement, Near-field imaging, Optical antenna, Plasmonics, Quantum Cascade Laser, Surface plasmon resonance.

1. INTRODUCTION

At the interface between two mediums having opposing signs of dielectric susceptibility (eg. Metal-dielectric), light can generate a collective motion of conductive electrons, called by surface plasmons (SP)[1]. The principle of surface plasmons has been extensively applied in many novel applications for example extraordinary optical transmission[2,3,4], label-free measurements of bio-molecular sensing [5,6], drug discovery [7,8], surface plasmon interference lithography [9]and spectroscopic applications [10].

By solving the Maxwell's equation in a planar film, the SP dispersion relationship is found to be:

[1] hmohseni@ece.northwestern.edu, 1-847-491-5412; www.bisol.northwestern.edu

Laser Beam Shaping XI, edited by Andrew Forbes, Todd E. Lizotte, Proc. of SPIE Vol. 7789, 77890L · © 2010 SPIE · CCC code: 0277-786X/10/$18 · doi: 10.1117/12.861451

$$k = \frac{\omega}{c}\sqrt{\epsilon_{eff}} \quad (1)$$

Where, k is the wave vector of the electromagnetic field propagation parallel to the interface between metal and dielectric, ω is the angular frequency of the incident field. ε_{eff} is the effective dielectric constant given by:

$$\epsilon_{eff} = \frac{\epsilon_d \epsilon_m}{\epsilon_d + \epsilon_m} \quad (2)$$

Where, ε_m and ε_d represent the dielectric constants for metal and dielectric respectively.

As formula (1) suggests, the angular momentum of SP is greater than the free space momentum of incident photon and thus exciting SP at the metal-dielectric interface requires special care. Previously, it has been achieved using two different coupling techniques – prism coupler [1] or grating coupler[11].

The familiar concepts of geometrical optics in the macroscopic world do not adequately describe light-particle interaction when the particle size becomes comparable to the wavelength of the incident light. In such condition, rigorous optical theories such as Mie theory [12] address the solution of Maxwell equation with full complexity of light-particle interaction.

Mie theory suggests that a collective charge oscillation i.e. SP gets induced when an incident electromagnetic field interacts with the target nano particle. Moreover the oscillating frequency matches with the frequency of incident field. For such small particle size, SP is dipolar[13]. It induces the charge accumulation process at the two ends of the nano particle with opposite polarity. The accumulated charge generates strong electric field in the near field region of the nano particle due to coulomb interaction. Such phenomena expand the realm of geometric optics to focus radiant visible and infrared light down to nanometric length scale much smaller compared to its wavelength.

In the past decade, there has been considerable amount of research on optical antennas due to its novel photonic application including chemical[14,15] and thermal sensors[16,17], near-field microscopy[18,19], nanoscale photodetectors[20] and plasmonic devices[21,22,23]. Like RF antenna, optical antennas are resonant structures responding to specific wavelengths through both the geometrical and material characteristics of the antenna as well as the surrounding environments[24,25,26]. Though both optical and RF have fundamental application in controlling radiation pattern, there do exist some basic differences. For example, radio frequency (RF) antenna designs[27] wholly focus on optimization of far-field characteristics in order to obtain better long distance transmission and reception performance. In contrast optical antenna emphasize on the near field behavior because the enhancement decays rapidly with distance. Further, the primary challenge of dimensional mismatch between the wavelength and the emitter/receiver (e.g. molecules) for optical antenna is met by improvement in near-field coupling instead of using a feed line as in the RF case.

Significant works related to optical antenna in visible spectrum[28] has been previously demonstrated. Recently there has been an added interests in infrared (IR) optical antenna due to relatively ease of structural fabrication compared to visible range, and more importantly the great technological need for its potential applications in chemical spectroscopy, remote sensing, ultrafast IR and THz transient detection[29,30]. Many of the demonstrated infrared optical antennas were designed based on an external IR laser source[31,32,33]. Integration of optical antenna along with an IR source was far-reach for a long time due to the absence of any efficient laser source in this optical regime (2-20 μm) till the field of Quantum Cascade Laser matured significantly in the last decade. Since its first demonstration[34] in 1994, QCL – a unipolar semiconductor laser[35] which works on the principle of intersubband transitions, showed watt level power performance at room temperature[36]. Group lead by Fredrico Capasso at Harvard University, first demonstrated a fully integrated mid-infrared optical antenna based on QCL and showed a strong near field localization[37,38,39,40,41,42]. Such optical antenna showed great promise in microscopic application below diffraction limit. The usefulness can be extended further to chemical and bio sensing application if composite material (multilayered) is used instead of single metal as optical antenna element as it paves the way to functionalize different layers.

Here, we demonstrate a metal-dielectric-metal (MDM) based nanorod antenna design, where surface plasmon waves at two metal interfaces get coupled by the sandwiched dielectric medium. In comparison to a metal nanorod antenna, such a design promises stronger light enhancement. Furthermore, as a result of higher number of geometrical singularities or sharp edges present in the MDM structure, it can increase the number of regions with local hot spots making it extremely useful for bio-sensing applications[43,44]. Moreover the design is superior to a

single metal nanorod because it opens up the possibility of use it for many bio-sensing applications where different probe molecules can be attached to different layers of the same nanorod[45].

2. SIMULATIONS

To analyze the performance of our MDM antenna compared to metal nanorod antenna, we first simulated the structure using commercially available 3d FDTD software, Lumerical. All material data used in the simulation, other than the laser region, is from ref 46. The refractive index of the laser material is chosen to be 3.2, which is the weighted average of the refractive index of the active region,$In_{0.44}Al_{0.56}As/In_{0.6}Ga_{0.4}As$. The simulated structure has a 100nm buffer silicon dioxide followed by the metal-dielectric-metal antenna. A schematic diagram of the simulated structure is shown in the inset of Figure 1. An optical TM polarized plane wave with central wavelength around 5.97um and it is used as the source for all performed FDTD simulations.

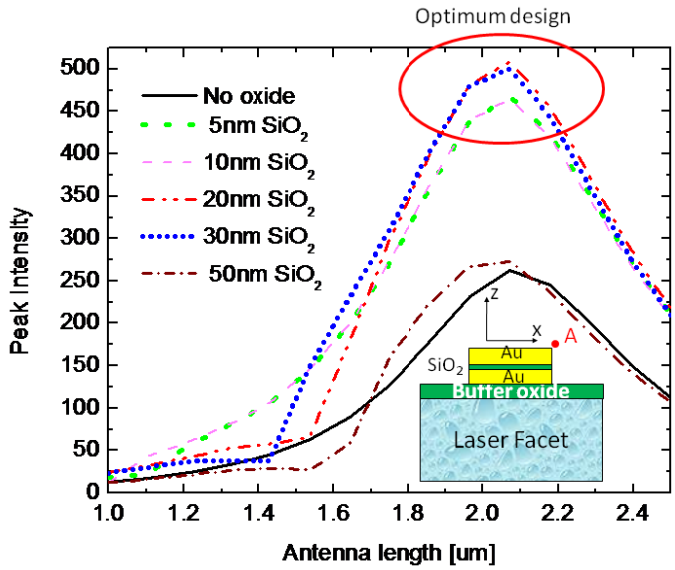

Figure 1 - (color online) FDTD simulation showing the peak intensity enhancement for varying the silicon dioxide thickness while keeping the total thickness of the structure to be 170nm. Inset: Schematic diagram of the simulation structure, where the "A" represents the position of the sampling point.

At resonance, surface charge is accumulated at the end of each nanorod and it is maximized at the gap between two closely placed nanorods due to capacitive coupling. The accumulated charge leads to large electric field intensity enhancement at its vicinity. Peak electric field enhancement is plotted against varying lengths of the nanorod antenna (Figure 1). In the simulations, we varied the SiO_2 thickness from 0, 5, 10, 20, 30 to 50 nm, while keeping the total structure thickness to be 170nm. It can be seen that by increasing the SiO_2 thickness from 5 to 10nm, the average intensity is enhanced. It is maximized at a thickness of 20nm and decreases at an oxide thickness of 30nm.

The physics behind the MDM single nanorod design can be well understood by an analogous LC circuit[47], where each metal layer is represented by identical inductors (L) and the sandwiched dielectric between them as a capacitor (C). Also two of the nanorods create a capacitor, C_a, outside the dielectric region. In Figure 2, a schematic diagram of the equivalent optical circuit is shown. All the optical circuit elements are in parallel and they form a coupled LC circuit with a resonance frequency $\omega^2 \sim (C+C_a)/L.C.C_a$. When the input signal frequency is close to ω, a strong resonance occurs. With a fixed lasing frequency, as used in our design, the thickness parameters can be tuned with the resonance frequency, making the device uniquely different from the single metal nanorod antenna.

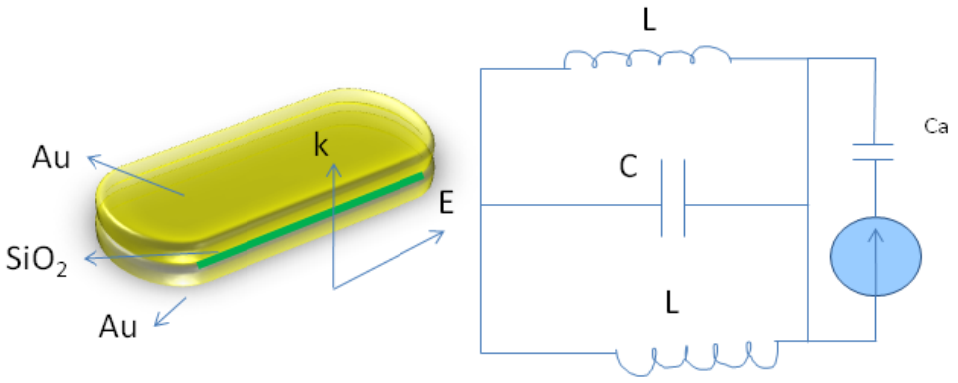

Figure 2 - Schematic diagram showing the MDM single nanorod antenna and the equivalent optical circuit for this structure.

At the resonant lengths, L=2.0um for the MDM antenna and L=2.05um for metal antenna, the absolute value of electric field distribution along as the z-direction is plotted in Figure 3(a) - (b) respectively. The local electric field enhancement can be a good figure of merit to compare the plasmon coupling efficiency between single metal and MDM designs. The MDM nanorod antenna has nearly 3 times higher enhancement at the top metal surface as compared to the single nanorod antenna (Figure 3 (c)). This field enhancement can be attributed to the increased plasmon coupling efficiency in the presence of the sandwiched SiO_2.

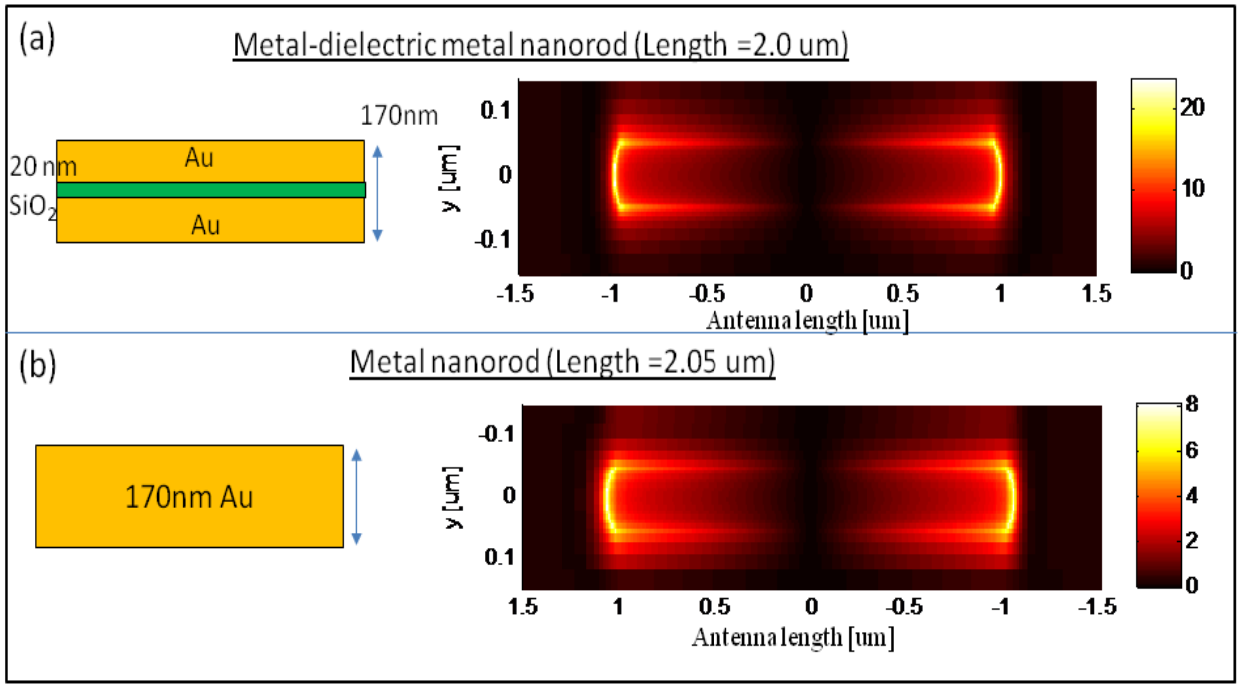

Figure 3 – (a) Schematic diagram showing MDM ($Au/SiO_2/Au$; 75/20/75nm) nanorod antenna design and the corresponding Ez field distribution at the top of the metal surface at a resonant length of 2.0um. (b) Schematic diagram showing metal antenna design and the corresponding Ez field distribution at the top of the metal surface at a resonant length of 2.05um.

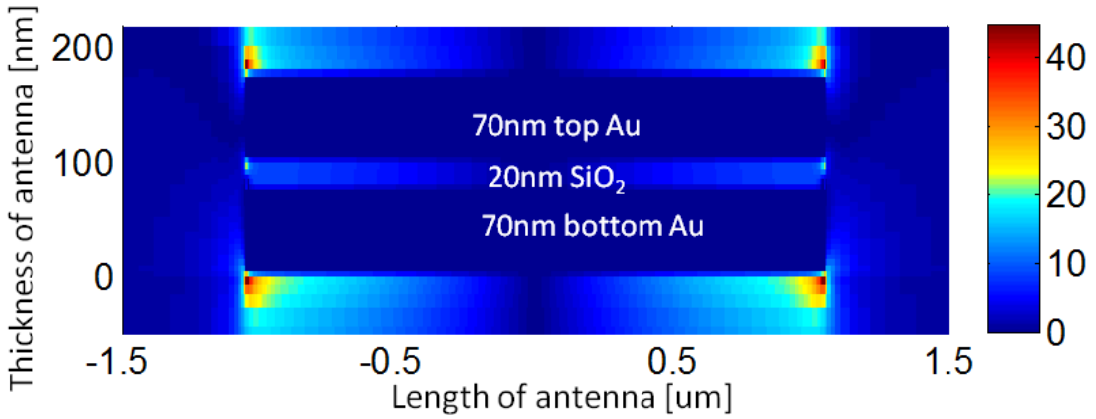

Figure 4 – Cross-sectional view of the MDM (Au/SiO_2/Au; 70-20-70nm)nanorod antenna at resonant length of 2um, where the color bar represents the total E-field.

The local electric field distribution for the MDM antenna at resonant length of 2um is shown in Figure 4. The picture shows the simulated hot spot regions where the electric field intensity gets enhanced.

From the simulation, the first order resonant length of the antenna is found to be L= (2.0±0.1) μm, which corresponds to a half integer multiple of the effective wavelength ($\lambda_{eff}= \lambda_0/n_{eff}$). At resonant condition, the peak intensity, at the two ends of the antenna, is found to be ~ 500 times the incident field intensity. A dipolar behavior can still persist away from resonant conditions but it is expected to show increasingly asymmetric field distribution[31] until charge accumulation gets completely faded.

3. EXPERIMENTAL SET-UP

The resolution of Fourier transform infrared microcopy (FTIR) can't exceed more than a few micrometer due to diffraction limitation. In contrast, apertureless near-field scanning optical microscopy (a-NSOM) offers spatial resolution up to few tens of nanometers and independent of any wavelength. The experimental set-up has been illustrated in Figure 5. The tip of an atomic force microscope (AFM) scans parallel to the surface normal of the antenna in tapping mode. Local electromagnetic field from the antenna structure is scattered by the AFM tip. Part of it gets transmitted through the laser cavity and collected by a mercury-cadmium telluride (MCT) detector after beam collimation.

The scattered signal possesses local field information. However, there is also scattering from the cantilever which produces a huge background noise. This background has been overcome by modulating the distance between the probe and the sample. At a small distance between the probe and sample, the apex signal gets hugely enhanced. There is also a contribution to the modulated signal from many other scattering centers along the probe shaft. But the signal contribution of the more distant ones can be effectively suppressed due to their rapid fading at larger distance from the sample[48,49]. Thus modulating the signal using AFM in tapping mode and then demodulating using a lock-in amplifier can give an excellent background suppressed near-field signal.

Due to selection rule for intersubband transition, QCL emits TM polarized light[50], where direction of the electric field is along the growth direction. The antenna structure is integrated on the facet of the QCL such that the antenna axis coincides with the direction of laser polarization. Such condition makes the antenna resonant with the incident laser frequency and enhances the near field. There is also a perturbation effect on the antenna near-field due to the presence of probing tip, but it can be suppressed by using dielectric tip instead of metal tip as been suggested in ref 51.

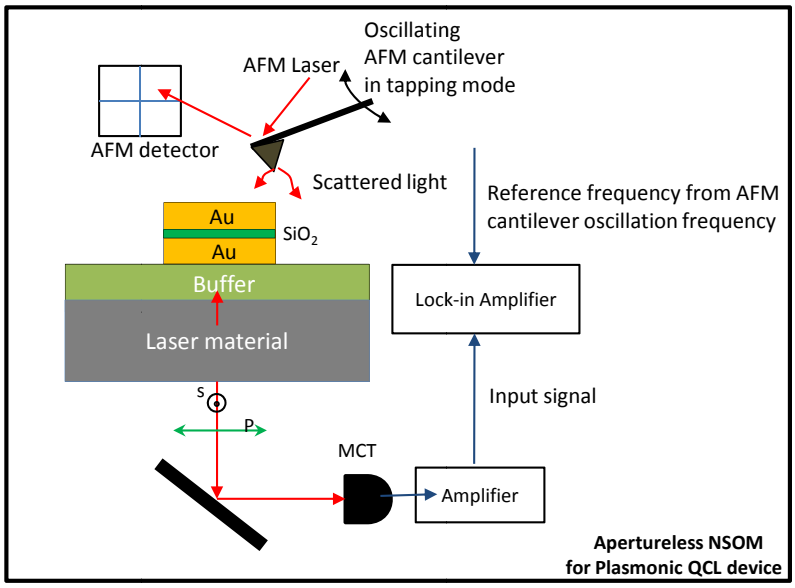

Figure 5 - Apertureless near-field optical microscope (a-NSOM) to probe near field intensity of optical antennas.

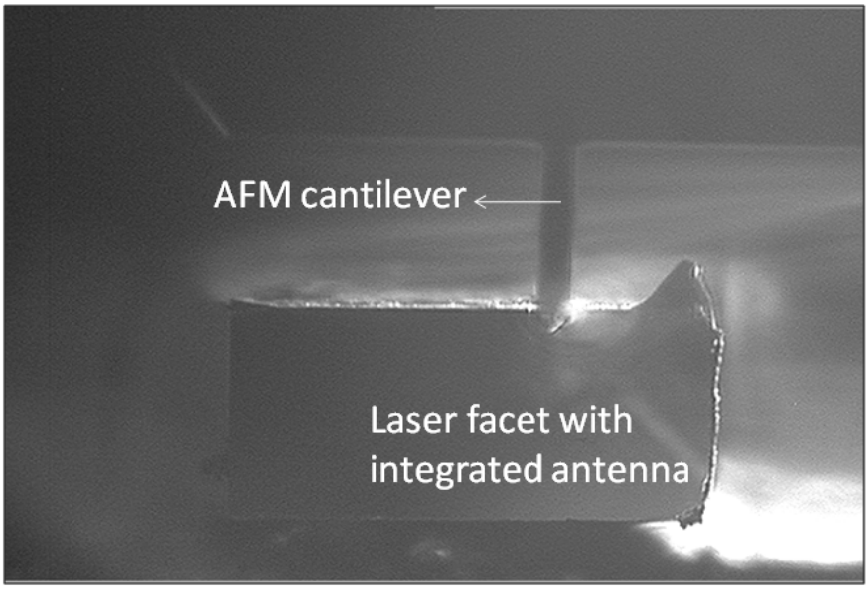

Figure 6 – Optical image showing the AFM tip scanning the facet of the QCL with integrated antenna.

The metal-dielectric-metal nanorods were fabricated on the facets of both an injectorless quantum cascade (I-QCL) laser and a conventional QCL laser, working at room temperature. I- QCL is based on $In_{0.365}Al_{0.635}As$ /$In_{0.66}Ga_{0.34.}$ The core design is similar to an earlier letter[52], but modified with higher strain (~3%) and doping density. It had already been reported that the I-QCL shows superior thermal performance with approximately 8 times lower rise in core temperature compared to conventional QCL with injector[53]. Conventional QCL is based on $In_{0.44}Al_{0.56}As/In_{0.6}Ga_{0.4}As$ with a core design as outlined in a previous letter[54]. The results described in this paper are based on devices fabricated on conventional QCL. Although, the fundamental physics of devices based on I-QCL is expected to be identical, other than the dimensional difference caused by difference in operation wavelengths of the two lasers.

The cleaved lasers were mounted on a c-mount and tested for current-voltage performance at room temperature. After initial characterization to verify the operation of the lasers, one facet of the device was coated with SiO_2/Au/SiO_2/Au (200/75nm/20nm/75nm) by ebeam evaporation using an Edwards FL 400. The single nanorod antenna designs were then fabricated on the coated facet of the lasers using a Focused Ion beam (Hellios FEI). Using the gallium ion beam at high voltage (30keV) and low current (48pA), a high precision of milling was achieved. After the patterning, current-voltage characteristics didn't incur any significant changes.

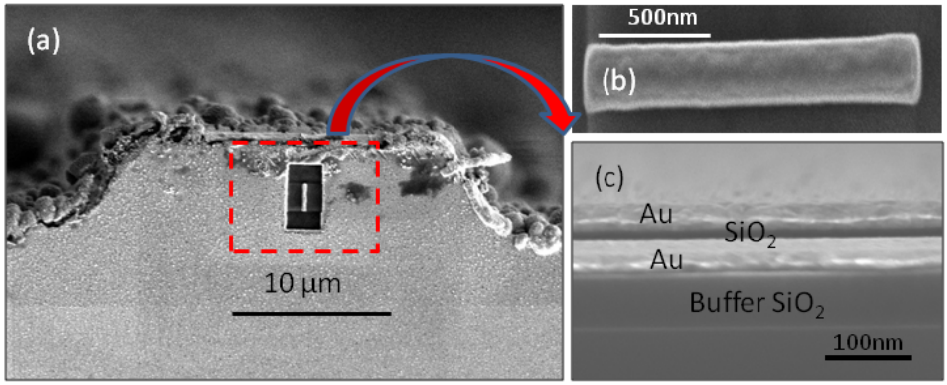

Figure 7 – (a) SEM image of the side view of Au-SiO_2-Au (75/20/75nm) coupled nanorod antenna (b) Top view of Au-SiO_2-Au (75/20/75nm) single nanorod antenna. (c) Side view of Au-SiO_2-Au (75/20/75nm) single nanorod antenna.

4. MEASUREMENT

Experimentally, nanorod on the laser facet was located using AFM scanning. Under laser in operation, the AFM tip-scattered near-field response is recorded simultaneously with the topography. When in plane incident field interacts with the MDM nanorod, conduction electrons in the metal respond with generating a surface Plasmon wave. For composite material based antenna surface Plasmon waves get generated at each interface between metal and dielectric.

During NSOM measurement, there are two components of scattered electric field, E_x (in-plane) and E_z (out-of plane), interacts with the oscillating AFM probe. Unlike in phase dipole oscillation as in E_x , the E_z field components at opposite ends of the nanorod oscillate out of phase with respect to each other by a relative angle $\varphi=\pi$. In Figure 8 (a) – (b), we show the near field image of Au-SiO_2- Au (75/20/75nm) single nanorod antenna , with a length of L=2.0µm, integrated on the facet of room temperature working QCL. The simulated dipolar pattern in Figure 8 (c) shows high near-field amplitude values at the rod extremities and zero amplitude at the center and it matches with the experimental result. The simulated $|E_z|$ component (Figure 8 (c)) and $|E_x|$ of the electric field (Figure 3(b)) shows clearly that we experimentally measure the E_z instead of E_x component of the electric field. Unlike interferometric NSOM[55,56,57], a-NSOM can't selectively measure two different components of E-field and thus only the significant component of the near field is expected to be recorded. As been described in ref 51, the electric field component parallel to the sample surface yields a relatively weak scattering signal compared to the component perpendicular to it. It is due to difference between their effective polarizability. Thus probing out-of-plane E_z component ideally suited for such measurement.

We have found a more intense spot at the left corner of the nanorod compared to the right (Figure 8 (b)). Similar observation has been reported in ref 32 and it is due to unsuppressed background noise. The line scans of topography and near field are shown in Figure 8 (d) – (e). The image distortions, as seen Figure 8 (a) – (b), is due to small sample drift and it is because the long acquisition time (~ 1 hour) for a-NSOM measurement.

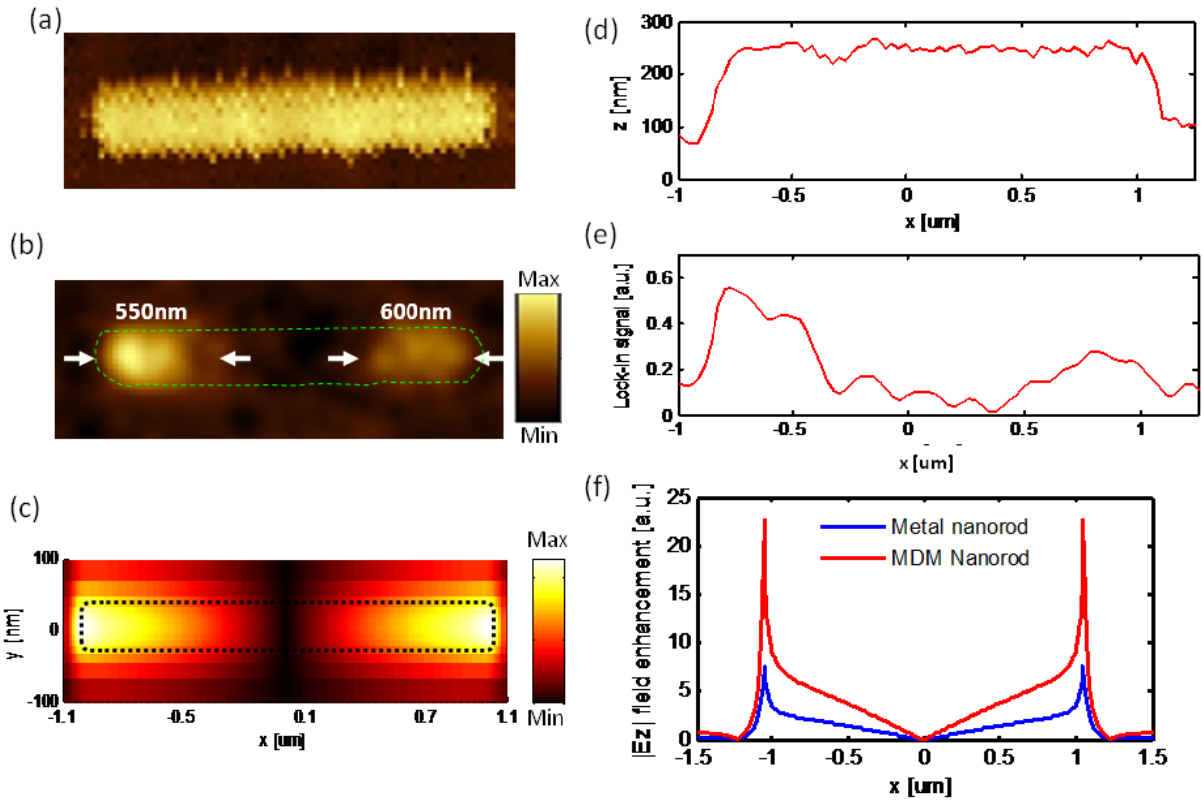

Figure 8 – (a) –(b) Topography and NSOM image of the Au-SiO_2-Au single nanorod antenna integrated on the facet of a room temperature working quantum cascade laser (c) Simulated $|E_z|$ for the MDM nanorod antenna. (d) – (e) Line scans for topography and NSOM measurement respectively (f) Comparison between the $|E_z|$ near field intensity for single metal (170nm Au) and MDM nanorod antenna. It shows that MDM antenna has > 3 times near field intensity enhancement.

5. DISCUSSION

During the NSOM measurement, the laser was operated at 1% duty cycle near the threshold voltage with an average power output of 100µW. The near-field images of the antenna were recorded with high pixel resolution and with a reduced scan speed of 0.1 line/s. The NSOM images show excellent agreement with the z-component of the simulated near field distribution. The full widths at half maximum of the two peak intensities at the edge of the antenna were found to be 550 and 600nm respectively (Figure 8). The spot is naturally confined along the short direction of the antenna width of 100nm. The generated power flux at each hot spot is calculated as the total operating laser power divided by number of spots and spot area. Neglecting any incurred optical losses the total power flux is calculated to be approximately 0.8nW/nm^2 per hot spot. Even at 1% of this value, there will be enough optical power to have an interaction with single molecules[58]. The measured peak intensities (Figure 8) at the two ends of the antenna are different because of possible non-uniformity of the top gold surface caused by FIB milling.

In conclusion, we have demonstrated near field scanning optical microscopy of a single nanorod antenna integrated on to the facet of a room temperature working QCL. The presented composite material based antenna designs can generate a very small optical spot size with power flux density in the order of nW/nm^2. Simulations have confirmed that its multilayered design can significantly increase this intensity enhancement. Such high power densities combined with multiple hot spot location on the same antenna will enable us to detect single molecule based on their unique vibrational signature.

6. ACKOWLEDGEMENT

This work was partially funded by NSF. The Focused Ion beam milling and SEM studies were performed in the (EPIC) (NIFTI) (Keck-II) facility of NUANCE Center at Northwestern University. NUANCE Center is supported by NSF-NSEC, NSF-MRSEC, Keck Foundation, the State of Illinois, and Northwestern University. The Materials Research Center (MRC) cleanroom facility at Northwestern University was used for ebeam evaporation.

[1] H. Raether. "*Surface plasmons on smooth and rough surfaces and on gratings*". (Springer. 1999)
[2] T.W. Ebbesen, H.J. Lezec, H. F. Ghaemi, T. Thio and P. A. Wolff. "*Extraordinary optical transmission through sub-wavelength hole arrays,*" Nature. **391**, 667 (1998)
[3] A.Lesuffleur,I. H. Im, N. C. Lindquist, S. H. Oh. "*Periodic nanohole arrays with shape-enhanced Plasmon resonance as real time biosensors,*" Applied Physics Letter. **90**, 261104 (2007)
[4] Y. Lie, J. Bishop, L. Williams, S. Blair and J. Herron. "*Biosensing based upon molecular confinement in metallic nanocavities,*" Nanotechnology **15**, 1368 (2004)
[5] C.T. Cambell and K.G. Him. "SPR microscopy and its applications to high-throughput analyses of biomolecular binding events and their kinetics," Biomaterials **28** (15), 2380-2392 (2007)
[6] S. Nie and S. R. Emory."*Probing single molecule and single nanoparticles by surface enhanced raman scattering,*" Science **275**, 1102 (1997)
[7] B. Liedberg, C. Nylander and I. Lunstrom. "*Surface plasma resonance for gas detection and biosensing,*" Sensor and Actuators **4**, 299 (1983)
[8] M.A. Cooper. "*Optical bio sensors in drug discovery,*" Nat. Rev. Drug Discovery **1**, 515 (2002)
[9] Z. Liu, J. M. Steele, W. Srituravanich, Y. Pikus, C. Sun and X. Zhang. Nano Letter. **5**, 1726 (2005)
[10] K. Kneipp, Y. Wan, H. Kneipp, L. T. Perelman, I. Itzkan, R. Dasari and M. S. Field. "*Single molecule detection using surface-enabled Raman scattering,*" Physical Review Letter. **78**, 1667 (1997)
[11] W.L. barnes, S. C. Kitson, T. W. Priest and J.R. Sambles. "*Photonic surfaces for surface Plasmon polaritons*" Journal of te optical society of America A – Optics image Science and vision. **14**, 1654-1661 (1997)
[12] G. Mie. "*Articles on the optical characteristics of turbid tubes, especially colloidal metal solutions,*" Annalen Der Physik, vol. **25**, 377-445 (1908)
[13] R. Marty, G. baffou, A. Arbouet, C. Girad and R. Quidant. "*Charge distribution inside complex plasmonic nanoparticles,*" Optics Express. Vol **18**, No 3 (2010)
[14] T.H.Taminiau, F. D. Stefani, F. B. Segerink abd N.F. van Hulst."*Optical antennas direct single-molecule emission,*" Nature Photonics **2**, 234-237 (2008)
[15] V.Giannini and J. A. Sanchez-Gil. "*Excitation and emission enhancement of single molecule fluorescence through multiple surface-plasmon resonances on metal trimer antennas,*" Optics Letter **33**, 899-901 (2008)
[16] P. Krenz, J. Alda and G. Boreman. "*Orthogonal infrared dipole antenna,*" Infrared Physics Technology. **51**, 340-343 (2008)
[17] C. Fumeaux, M. A. Gritz, I. Codreanu, W. L. Schaich, F. J. Gonzalez and G. D. Boreman. "*Measurement of the resonance lengths of infrared dipole antennas,*" Infrared Physics Technology **41**, 271-281 (2000)
[18] N. Yu, E. Cubukcu, L. Diehl, M. A. Belkin, K. B. Crozier, F. Capasso, D. Bour, S. Corzine and G. Hofler. "*Plasmonic quantum cascade laser antenna,*" Applied Physics Letter **91**, 173113 (2007)
[19] A.Cvitkovic, N. Ocelic, J. Aizpurua, R. Guckenberger and R. Hillenbrand. "*Infrared imaging of single nanoparticles via strong field enhancement in scanning nanogap,*" Physical Review Letter **97**, 060801 (2006)
[20] L. Tang, S. E. Kocabas, S. Latif, A. K. Okyay, D. S. Ly-Gagnon, K. C. Sarswat and D. A. B. Miller. "*Nanometre-scale germanium photodetector enhanced by a near-infrared dipole antenna,*" Nature Photonics **2**, 226-229 (2008)
[21] M. Pelton, J. Aizpurua and G. Bryant. "*Metal-nanoparticle plasmonics*". Laser Photon. Rev. **2**, 135-159 (2008)
[22] J.N. Farahani, D. W. Pohl, H.J. Eisler and B. Hecht. "*Single quantu dot coupled to a strong scanning optical antenna: A tunable super emitter*". Physical Review Letter **95**, 017402 (2005)
[23] S. D. Lie, M. T. Cheng, Z. J. yang and Q. Q. Wang."*Surface plasmon propagation in a pair of metal nanowires coupled to nanosized optical emitter*" Optics Letter **33**, 851-853 (208)
[24] F. Neubrech, T. Kolb, R. Lovrincic, G. Fahsold, A. Pucci, J. Aizpurua, T. W. Cornelius, M. E. Toimil-Molares, R. Neumann and S. karim. "*Resonances of individual metal nanowires in the infrared*". Applied Physics Letter **89**, 253104 (2006)

[25] J.Merlein, M. Kahl, A. Zuschlag, A. Sell, A. Halm, J. Boneberg, P. Leiderer, A. Leitenstorfer and R. Bratschitsch. "*Nanomechanical control of an optical antenna*" Nature Photonics **2**, 230-233 (2008)
[26] K.B.Crozier, A. Sundaramurthy, G.S. Kino and C. F. Quante. "*Optical antennas: Resonators for local field enhacement*". Journal of Applied Physics **94**, 4632-4642 (2003)
[27] F.J.Gonzalez and G.D.Boreman. "*Comparison of dipole, bowtie, spiral and log-periodic IR antennas*" Infrared Phys. Technol. 46, 418-428 (2005)
[28] R.D. Grober, R. J. Schoelkopf and D.E. Prober, "*Optical antenna: Towards a unity efficiency near-field optical probe*" Applied Physics Letter. **70**, 1354 (1997)
[29] E. R. Encina and E. A. Coronado. "*Resonance conditions for multipole plasmon excitations in noble metal nanorods,*" Journal Physical Chemistry C **111**, 16796 (2007)
[30] J.Aizpurua, G. W. Bryant, L. J. Richter, F. J. Garcia de Abajo, B. K. Kelley and T. Mallouk. "*Optical properties of coupled metallic nanorods for field-enhanced spectroscopy,*" Physical Review B **71**, 235420 (2005)
[31] R. L. Olmon, P. M. Krentz, A. C. Jones, G. D. Boreman and M. B. Raschke. "*Near-field imaging of optical antenna modes in the mid-infrared,*" Optics Express vol **16**, No 25 (2008)
[32] M. Schnell, A. G. Etxarri, A. J. Huber, K. B. Crozier, A. Borisov, J. Aizpurua and R. Hillenbrand. "*Amplitude and phase-resolved near field mapping of infrared antenna modes by transmission mode scattering type near filed microscopy*," Journal of Physical Chemistry Vol **114**, No 16 (2010)
[33] M. Rang, A. C. Jones, F. Zhou, Z. Y. Li, B. J. Wiley, Y. Xia and M. B. Raschke. "*Optical near-field mapping of plasmonic nanoprisms*" Nano Letter Vol **8** , No 10 (2008)
[34] J. Faist**,** F. Capasso , D. L. Sivco , C. Sirtori , A. L. Hutchinson , and A.Y. Cho."*Quantum Cascade Laser*" Science **264**, 553 (1994)
[35] Y.Bai, S. Slivken , S. Kuboya , S. R. Darvish and M. Razeghi. "*Quantum cascade laser that emits more light than heat,*"Nature Photonics **4**, 99 (2010)
[36] Y Bai, S Slivken, SR Darvish, M Razeghi. "Room *temperature continuous wave operation of quantum cascade laser with 12.5% wall-plug efficiency*," Applied Physics Letter **93**, 021103 (2008)
[37] E. Cubukcu, E.A. Kort, K. B. Crozier and F. Capasso. "*Plasmonic laser antenna,*" Applied Physics Letter **99**, 093120 (2006)
[38] N. Yu, E. Cubukcu, L. Diehl, M. A. Belkin, K. B. Crozier, F. Capasso, D. Bour, S. Corzine, G. Hofler. "*Plasmonic quantum cascade laser antenna,*" Applied Physics Letter 91, 173113 (2007)
[39] N. Yu, E. Cubukcu, L. Diehl, D. Bour, S. Corzine, J. Zhu, G. Hofler, K. B. Crozier, and F. Capasso "*Bowtie plasmonic cascade laser antenna,*" Optics Express **15**, 13272 (2007)
[40] E. Cubukcu, N. Yu, E. J. Smythe, L. Diehl, K. B. Crozier and F. Capasso. "*Plasmonic laser antenna and related devices,*" IEEE Journal of Selected Topics in Quantum Electronics **14**, 1448 (2008)
[41] N. Yu, R. Blanchard, J. Fan, Q. J. Wang, C. Pflugl, L. Diehl, T. Edamura, M. Yamanishi, H. Kan and F. Capasso *"Quantum cascade lasers with integrated plasmonic antenna-array collimator,"* Optics Express **16**, 19447 (2008)
[42] N. Yu, R. Blanchard, J. Fan, Q. J. Wang, C. Pflugl, L. Diehl, T. Edamura, S. Furuta, M. Yamanishi, H. Kan and F. Capasso . "*Plasmonics for laser beam shaping,*" IEEE Transactions on Nanotechnology **9**, 11 (2010)
[43] K. H. Su, Q. H. Wei and X. Zhang. "*Tunable and augmented Plasmon resonances of Au/SiO_2 /Au nanodisks,*" Applied Physics Letter **88**, 063118 (2006)
[44] A. Dmitriev, T. Pakizeh, M. Kall and D. S. Sutherland. "*Gold-Silica-Gold nanosandwiches " Tunable Biomodal Plasmonic Resonators*, " Small Vol **3** , 294-299 (2007)
[45] K. H. Su, S. Durant, J. M. Steele, Y. Xiong, C. Sun and X. Zhang. "*Raman enhancement factor of single tunable nanoplasmonics resonator,*" Phys. Chem. B **110**, 3964 (2006)
[46] E. D. Palik. "*Handbook of Optical constants of solids* ". (Academic Press, New York, 1985)
[47] N. Engheta. "*Circuits with light at nanoscales: optical nancircuits inspired by metamaterials,*" Science **317**, 1698 (2007)
[48] B. Knoll and F. Keilmann. "*Enhanced dielectric contrast in scattering-type scanning near-field optical microscopy*". Optics Communication **182**, 321 (2000)
[49] R. Hillenbrand, B. Knoll and F. Keilmann."*Pure optical contrast in scattering-type scanning near-field microscopy,*" Journal of Microscopy **202**, 77-83 (2000)
[50] H. C. Liu. "*Intersubband transition in Quantum wells: Physics and device application II*" Academic Press (1999)
[51] R. Rang, A. C. Jones, F. Zhou, Z.Li, B. J. Wiley, Y. Xia and M. B. Raschke. "*Optical Near0field mapping of plasmonic nanoprisms,*" Nano Letter **8**, 3357-3363 (2008)

[52] S. Katz, A. Friedrich, G. Boehm, M.C.Amann. "*Continious wave operation of injectorless quantum cascade lasers at low temperatures,*" Applied Physics Letter **92**, 181103 (2008)
[53] D. Dey, W. Wu, O. G. Memis and H. Mohseni. "*Injectorless Quantum cascade laser with low voltage defect and improved thermal performance grown by metal-organic chemical vapor deposition,*". Applied Physics Letter **94**, 081109 (2009)
[54] L.Diehl,D. Bour, S. Corzine, J. Zhu, G. Hofler, M. Loncar, M. Troccoli and F. Capasso. "*High-temperature continous wave operation of strain-balanced quantum cascade lasers grown by metal organic vapor-phase epitaxy,*"Applied Physics Letter **88**, 201115 (2006)
[55] M. Schnell, A. Garcia-Etxarri, A. J. Huber, K. Crozier, J. Aizpurua and R. Hillenbrand. "*Controlling the near-field oscillations of loaded plasmonic nanoantennas,*" Nature Photonics **3**, 287(2009)
[56] J. Dorfmuller, R. Vogelgesang, R. T. Weitz, C. Rockstuhl, C. Etrich, T. Pertsch, F. Lederer and K. Kern. "*Fabry-perot resonance in one-dimensional plasmonic nanostructures,*" Nano Letter **9**, 2372 (2009)
[57] R . L. Olmon, P. M. Krenz, A. C. Jones, G. D. Boreman and M. B. Raschke. "*Near-field imaging of optical antenna modes in the mid-infrared,*" Optics Express **16**, 25 (2008)
[58] M. F. Garcia-Parajo. "*Optical antenna focusing in on biology*," Nature, **2**, 201 (2008)